Anal Bioanal Chem (2007) 387:1669–1677
DOI 10.1007/s00216-006-0892-5

ORIGINAL PAPER

Classification of malignant gliomas by infrared spectroscopic imaging and linear discriminant analysis

Christoph Krafft · Stephan B. Sobottka · Kathrin D. Geiger · Gabriele Schackert · Reiner Salzer

Received: 29 June 2006 / Revised: 25 September 2006 / Accepted: 2 October 2006 / Published online: 14 November 2006

Abstract Infrared (IR) spectroscopy provides a sensitive molecular fingerprint for tissue without external markers. Supervised classification models can be trained to identify the tissue type based on the spectroscopic fingerprint. Infrared imaging spectrometers equipped with multi-channel detectors combine the spectral and spatial information. Tissue areas of 4×4 mm^2 can be analyzed within a few minutes in the macroscopic imaging mode. An approach is described to apply this methodology to human astrocytic gliomas, which are graded according to their malignancy from one to four. Multiple IR images of three tissue sections from one patient with a malignant glioma are acquired and assigned to the six classes normal brain tissue, astrocytoma grade II, astrocytoma grade III, glioblastoma multiforme grade IV, hemorrhage, and other tissue by a linear discriminant analysis model which was trained by data from a single-channel detector. Before the model is applied here, the spectra are shown to be virtually identical. The first specimen contained approximately 95% malignant glioma regions, that means astrocytoma grade III or glioblastoma. The smaller percentage of 12–34% malignant glioma in the second specimen is consistent with its location at the tumor periphery. The detection of less than 0.2% malignant glioma in the third specimen points to a location outside the tumor. The results were correlated with the cellularity of the tissue which was obtained from the histopathologic gold standard. Potential applications of IR spectroscopic imaging as a rapid tool to complement established diagnostic methods are discussed.

Keywords Brain tumors · Astrocytic gliomas · FTIR imaging · Tissue classification

Abbreviations

H&E	hematoxylin and eosin
FPA	focal plane array
FT	Fourier transform
LDA	linear discriminant analysis
TFM	tissue freeze medium

Introduction

Two main types of tissue are found in normal brain, referred to as white and gray matter, which consist of nerve fibers and glial cells, and a combination of neurons and glial cells, respectively. The most frequent primary brain tumors are astrocytic gliomas that are derived from astrocytes, a certain class of glial cells. They are classified according to the World

C. Krafft · R. Salzer
Institute for Analytical Chemistry,
Dresden University of Technology,
01062 Dresden, Germany

S. B. Sobottka · G. Schackert
Clinic for Neurosurgery, University Hospital,
Dresden University of Technology,
Fetscherstr. 74,
01307 Dresden, Germany

K. D. Geiger
Department of Neuropathology, Institute for Pathology,
University Hospital Dresden, Dresden University of Technology,
Fetscherstr. 74,
01307 Dresden, Germany

Present address:
C. Krafft (✉)
Department of Materials and Natural Resources,
University of Trieste,
Via Valerio 2, 34127 Trieste, Italy
e-mail: ckrafft@units.it

Health Organization (WHO) into four grades with increasing malignancy [1]: pilocytic astrocytoma (grade I), diffuse astrocytoma (grade II), anaplastic astrocytoma (grade III), and glioblastoma multiforme (grade IV). The last two are called malignant gliomas. The classification is not trivial, since the morphology used to classify the tumors forms a histological continuum and a single tumor may encompass regions of different morphology and cellularity with the highest grade of malignancy being relevant for the final classification of the tumor and the resulting therapy. Rapid assessment of cryostat sections accompanying surgery are performed to obtain pathological diagnoses and to determine tumor margins. The latter are usually determined by magnetic resonance tomography before surgery, but they may deviate from the preoperative locations due to intraoperative brain shift or edema. Distinction between tumor and normal brain tissue is particularly important in neurosurgery in order to maximally resect tumor cells and to minimally affect brain function. Cryostat sections for intraoperative diagnosis are prepared from fresh frozen samples. They are stained by hematoxylin and eosin (H&E), and evaluated by a neuropathologist. However, such an expert is not always available. Furthermore, the quality and quantity of tissue specimens constitute in some cases a problem for an accurate diagnosis.

Infrared (IR) spectroscopy was suggested as a tool in clinical and diagnostic analysis to complement the existing methods because of its potential to probe tissue and cells at the molecular level. The progress of IR spectroscopy for diagnostic applications was reviewed recently [2–4]. Its advantages include that (i) it is rapid, as spectral data can be collected and interpreted within minutes by automated algorithms; (ii) it requires minimal sample preparation, as molecular vibrations probe the chemical composition and structural properties of tissue sections without external markers; and (iii) it is non-destructive, so the sample can be subjected to further analyses such as immunohistochemistry in order to confirm the findings.

IR imaging spectrometers combine the spectral with lateral information. The spectra are acquired in parallel by imaging the sample on a multi-channel detector and by collecting images for each spectral data point. Coupling IR imaging spectrometers with microscopes gives diffraction-limited resolution in the 5- to 10-μm range. This high resolution capability is required, e.g., to investigate single cells [5] and to resolve small details such as germinal centers in spleen tissues [6] or different cell types in squamous cell cervical carcinoma [7]. The instrumentation and other applications have recently been reviewed [8]. A consequence of the high resolution is that multiple images have to be collected and pooled to study extended samples which yields large data sets and requires longer acquisition times. An alternative is IR macroscopic imaging which images the sample without magnification onto the multi-channel detector and which can reduce total acquisitions times for tissue sections of 4×4 mm^2 down to minutes.

IR spectroscopic brain studies have been reported for multiple sclerosis plaques [9], scrapie infections of the central nervous system [10], and animal models exhibiting brain tumors [11, 12]. Our group initiated a research program to develop IR spectroscopy-based techniques for identification of the primary tumor of brain metastases [13, 14] and for classification of astrocytic gliomas using a combination of a genetic-guided spectral region selection with linear discriminant analysis (LDA) [15, 16]. The genetic algorithm selects in an iterative process a set of variables for the LDA classification. Another supervised multivariate model using variables based on the chemical composition and LDA classification was introduced to assign single IR spectra or IR maps to the six tissue types normal brain tissue, astrocytoma grade II, astrocytoma grade III, glioblastoma multiforme grade IV, hemorrhage, and leptomeninges [17]. As the latter classification model gave more correct assignments, it is applied here. In contrast to IR imaging, IR maps are registered sequentially by a single-channel detector which takes to our experience approximately 100 times longer, and therefore it is impracticable as a rapid screening technique. The current paper describes how the procedures which have been reported elsewhere [17] can be transferred to IR images of three cryosections from a new glioma patient using training data from another experiment and different detectors. The descriptions of the tissue classes are refined after comparison to the histopathologic gold standard. This study is a prerequisite before the methods can be applied in a clinical setting to a larger set of samples using IR spectroscopic imaging as a tool to diagnose cryostat sections accompanying surgery. Then neurosurgeons can utilize this information in order to optimize tumor resections.

Materials and Methods

Sample preparation

All experimental procedures were approved by the Human Ethics Committee of the Dresden University of Technology. Multiple tissue samples were obtained from a patient with a glioblastoma multiforme brain tumor undergoing surgery. Tissue was embedded in tissue freeze medium (TFM), snap frozen, and cryostat sections were prepared afterwards. Ten-μm thick cryosections were mounted on IR-transparent calcium fluoride slides, dried in air, and imaged by IR spectroscopy in transmission mode. Photographs of unstained sections were taken using an Olympus microscope IX70 with a digital camera accessory (Soft Imaging

Systems, Münster, Germany). Consecutive tissue sections were mounted on glass slides and stained by H&E for histopathologic assessment. Photographs of H&E-stained sections were taken using a Zeiss Axioplan 2 microscope with a Canon 300D digital camera.

IR macroscopic imaging

IR spectroscopic images were recorded using a Bruker FTIR spectrometer IFS66/S equipped with a mercury cadmium telluride (MCT)-based focal plane array (FPA) detector of 64×64 pixels (Bruker Optik, Ettlingen, Germany). Coupling to the macro chamber IMAC (Bruker) gave a field of view of 4×4 mm^2 with a lateral resolution of 63×63 μm^2 per pixel. If the sample size exceeded 4×4 mm^2, multiple IR images were recorded by moving the sample using a manual stage. In contrast to the Hyperion microscope of the FTIR imaging spectrometer (Bruker), the sample stage in the macrochamber is not motorized. The FTIR spectrometer and the sample chamber were continually purged by dried air from air purifiers. Images of 4,096 IR spectra at 4-cm^{-1} spectral resolution were acquired by coadding 19 interferograms by the OPUS software (Bruker) operating the FPA in continuous scan mode. Recording time took approximately 4 min per image. Ratios of the single-beam spectra of each sample IR image against the spectra of a background IR image of neat calcium fluoride slides were obtained and converted to absorbance.

Data preprocessing

Data pretreatment was performed by routines written in-house under a MatLab platform (The Matworks, Natick, MA, USA). Different spectral backgrounds and offsets were corrected by subtracting multi-point baselines. Baseline points were selected near 950, 1,150, 1,480, 1,750, 2,800, 3,000, and 3,800 cm^{-1}. Spectra with intensities below 0.15 absorbance units were removed from further analysis because they mainly originate from holes and fissures in tissue sections and they have low "signal to noise" ratios.

Supervised classification by linear discriminant analysis

Band intensities at 2,850, 1,655, 1,545, 1,450, and 1,230 cm^{-1} were determined, and band ratios 2,850/1,655, 1,545/1,655, and 1,230+1,450/1,655 were calculated, which describe the six classes normal brain tissue, astrocytoma grade II, astrocytoma grade III, glioblastoma multiforme, hemorrhage, and other tissue. In the context of glioblastoma multiforme (grade IV), astrocytoma grades II and III are used as descriptive terms delineating the cellularity and morphological appearance of tumor areas in analogy to the morphological parameters used for WHO grading. However, they are not identical with the respective WHO classification. The spectral features were selected as descriptors because the band at 1,655 cm^{-1} is the most intense protein band, the band at 2,850 cm^{-1} is the second most intense lipid band which is, however, less affected by overlapping bands than the most intense band at 2,922 cm^{-1}. The band at 1,545 cm^{-1} has been recognized as a marker for hemoglobin, and the bands at 1,230 and 1,450 cm^{-1} as markers for other tissue such as leptomeninges. Eighteen spectra—three of each class—of specimens with known diagnosis were used to train a supervised classification model based on linear discriminant analysis, LDA. The spectra correspond to (1) the mean spectrum of the tissue class, (2) the spectrum with the minimum value of the descriptor, and (3) the spectrum with the maximum value of the descriptor. The training data were completely independent as they were selected from different specimens and they were collected by the optional MCT single-channel detector of the microscope coupled to the Bruker FTIR spectrometer IFS66/S. More details have been published previously [17]. The algorithm taken from the "Discrim Toolbox" calculates (K−1) discriminant functions which optimally separate K classes [18]. The classification model was applied to IR images from new samples as test objects and the resulting class memberships were color coded so that color-coded images could be assembled for visualization.

Results and discussion

Figure 1 shows an overlay of IR spectra from identical locations of normal brain tissue and of an astrocytic glioma brain tumor. The spectra recorded by the single-channel MCT detector and by the FPA detector are virtually identical

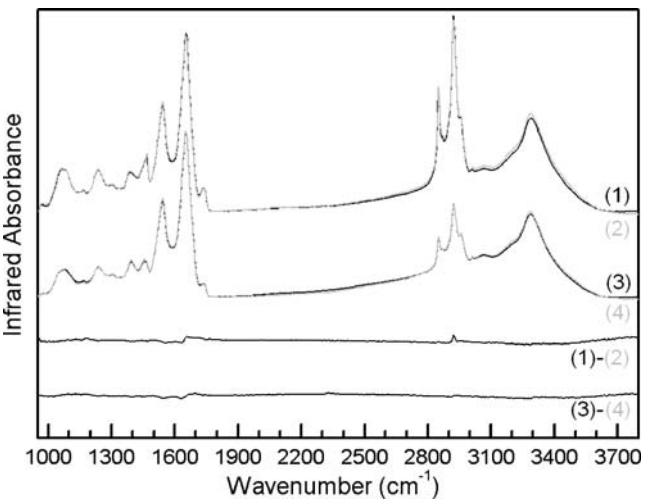

Fig. 1 Overlay of IR spectra recorded from two locations by the single-channel detector (*black traces 1*, *3*) and by the FPA detector (*gray traces 2*, *4*). Difference spectra (*traces 1–2* and *traces 3–4*) indicate that the spectra are virtually identical

after baseline correction. The difference spectra reveal only minimal deviations which are much smaller than the differences between tissue classes (see below). This observation constitutes the basis that the classification model which was developed by using data from the single-channel detector can be applied to data from the FPA multi-channel detector.

Figure 2 compares the photomicrograph of an unstained tissue section (a) with the color-coded IR images based on the LDA classification model (b). As the sample size was approximately 7.1×5.3 mm^2, two IR images were acquired. Four images would have been required to assess the whole cryosection. However, the top left and bottom right parts only encompass a minor portion of the sample, so two images of the main portion were acquired in order to save time. The majority of IR spectra were classified to glioblastoma multiforme (top 67%, bottom 53%) and to astrocytoma grade III (top 27%, bottom 43%). This means that on average 95% of the tissue section was assigned to malignant gliomas with the remaining spectra assigned to hemorrhage, to astrocytoma grade II near the tissue margins, and to other tissue. Comparison with the unstained tissue section reveals that the last class corresponds to

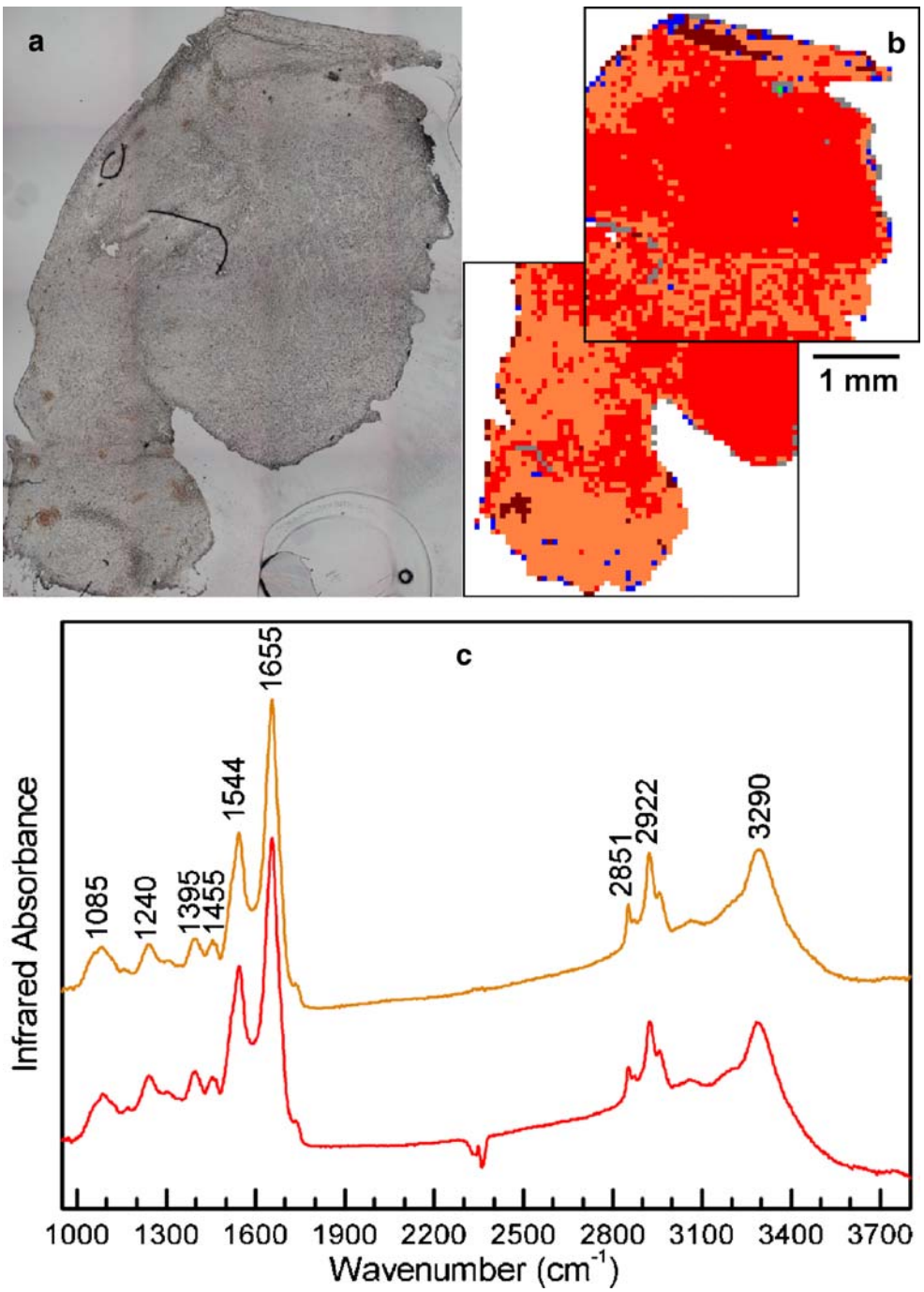

Fig. 2 Unstained cryosection of brain tissue (**a**), IR images (**b**), and single IR spectra of the main tissue classes glioblastoma multiforme and astrocytoma grade III (**c**). The *color coding* represents the class assignments of a LDA model: glioblastoma multiforme (*red*), astrocytoma grade III (*orange*), astrocytoma grade II (*blue*), normal tissue (*green*), hemorrhage (*brown*), and other tissue (*gray*). The spectra are normalized to equal intensities at 1,655 cm^{-1} and shifted to avoid overlap

impurities. Another example for impurities will be presented below.

Single IR spectra which represent the dominant tissue classes astrocytoma grade III (orange trace) and glioblastoma multiforme (red trace) are displayed in Fig. 2c. Main spectral contributions are assigned to proteins (1,395, 1,455, 1,544, 1,655, and 3,290 cm^{-1}) and lipids (1,085, 1,240, 2,851, and 2,922 cm^{-1}). After normalization of the

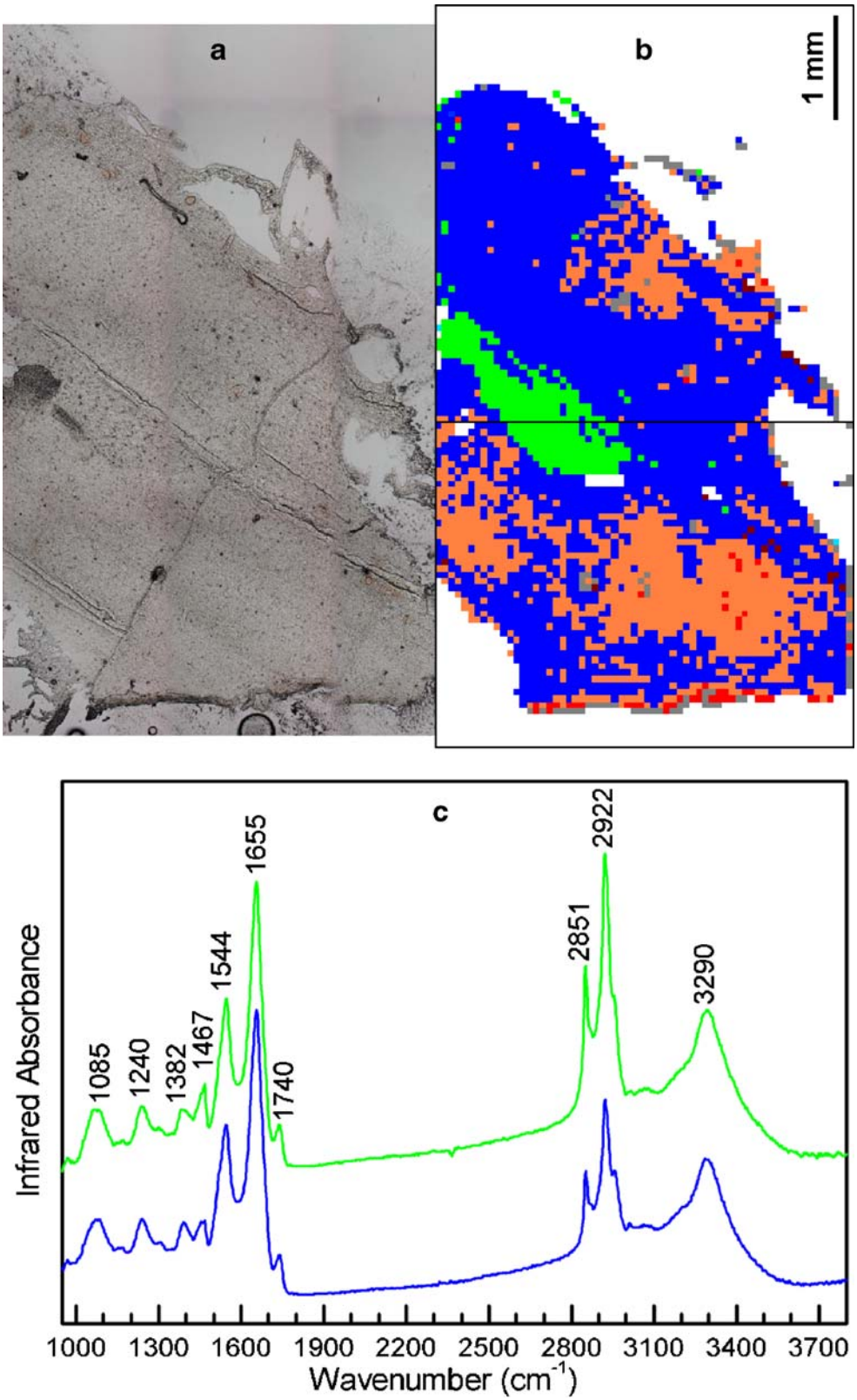

Fig. 3 Unstained cryosection of brain tissue (**a**), IR images (**b**), and single IR spectra of the tissue classes astrocytoma grade II and normal tissue (**c**). The *color coding* represents the class assignments of a LDA model: glioblastoma multiforme (*red*), astrocytoma grade III (*orange*), astrocytoma grade II (*blue*), normal tissue (*green*), hemorrhage (*brown*), and other tissue (*gray*). The spectra are normalized to equal intensities at 1,655 cm^{-1} and shifted to avoid overlap

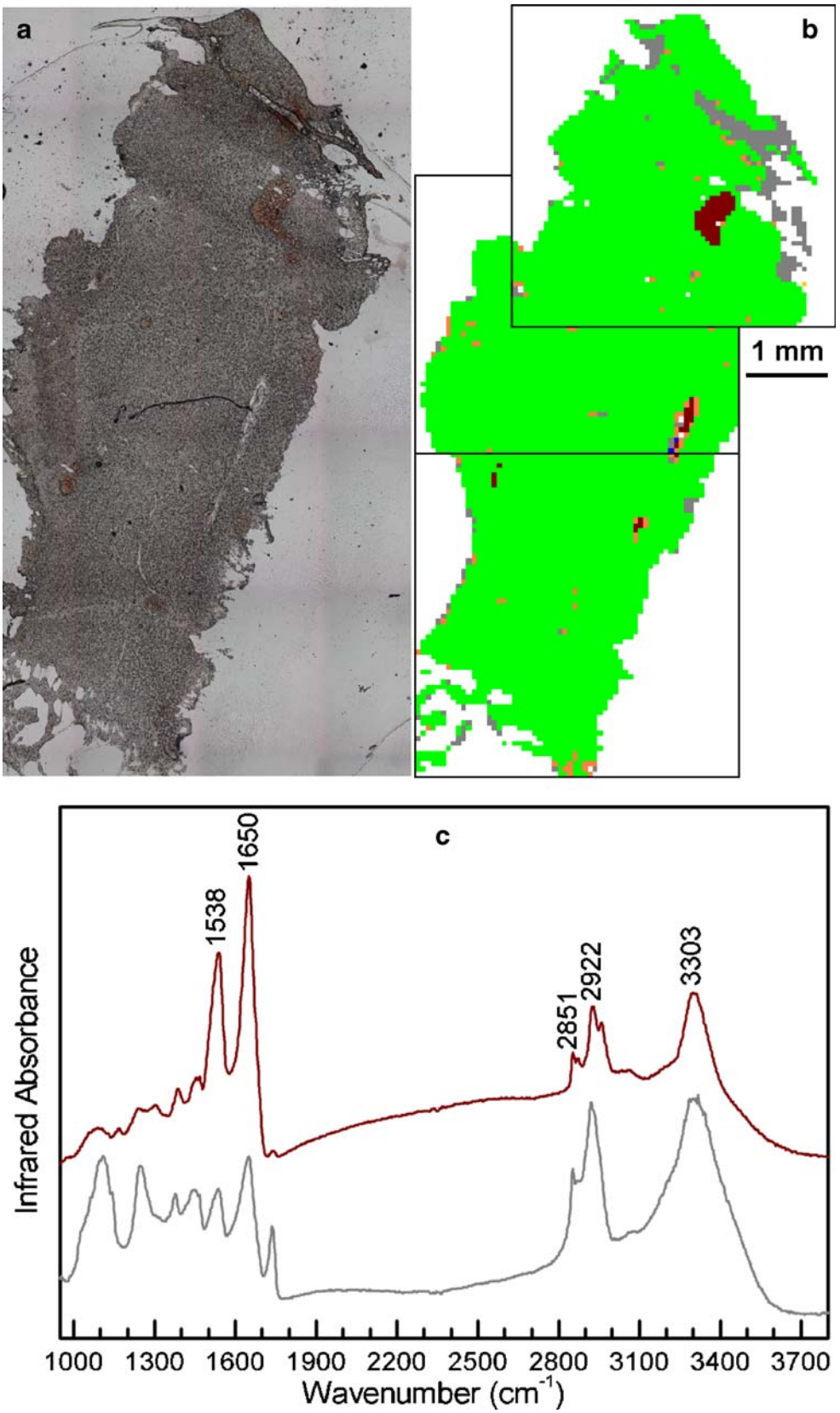

Fig. 4 Unstained cryosection of brain tissue (**a**), IR images (**b**), and single IR spectra of the tissue classes hemorrhage and other tissue (**c**). The *color coding* represents the class assignments of a LDA model: glioblastoma multiforme (*red*), astrocytoma grade III (*orange*), astrocytoma grade II (*blue*), normal tissue (*green*), hemorrhage (*brown*), and other tissue (*gray*). Spectra are shifted to avoid overlap

IR spectra to equal intensities at 1,655 cm^{-1} which compensates for slight differences in sample thickness, the most intense variances are found at 2,851 and 2,922 cm^{-1}. Consequently, the descriptor 2,851/1,655 cm^{-1} representing the lipid to protein ratio decreases from 0.14 (orange trace) to 0.11 (red trace). They coincide with the values reported earlier for astrocytoma grade III and glioblastoma multiforme, respectively [19]. The decrease of the lipid content in astrocytic gliomas was confirmed by other authors in an animal model [12]. As most lipids have been washed out from brain tissue during deparaffinization by organic solvents, this constituent could not be detected as a diagnostic parameter in a related animal study [11]. Other variances between both IR spectra in Fig. 2c were small. Spectral contributions from TFM were not detected which is consistent with TFM not penetrating into the tissue.

The 6×4-mm^2 sample area which is shown in Fig. 3a was studied by IR imaging. The IR images in Fig. 3b contain two new tissue classes, which are assigned by the LDA model to astrocytoma grade II (top 76%, bottom 50%) and to normal tissue (top 8%, bottom 7%). In addition, regions of astrocytoma grade III are present (top 12%, bottom 34%). Bands of lipids (1,085, 1,240, 1,467, 1,740, 2,851, 2,922 cm^{-1}) and cholesterol (1,382 cm^{-1}) increase in IR spectra of astrocytoma grade II (blue trace, Fig. 3c) and are maximum in IR spectra of normal brain tissue (green trace, Fig. 3c). The descriptor 2,850/1,655 for the lipid to protein ratio increases to 0.26 and 0.50, which also coincide with the previously reported values for astrocytoma grade II and normal brain tissue, respectively [19].

The cryosection size of 9.6×5.3 mm^2 required to record three IR images (Fig. 4a). The LDA model assigned more than 90% of spectra in each IR image to non-tumor tissue (Fig. 4b). In the top IR image two additional tissue classes are evident, which are assigned to hemorrhage (brown) and other tissue (gray). The spectral properties of both classes deviate from those of normal tissue or tumor. Representative IR spectra of these classes are shown in Fig. 4c. Minimum intensities of lipid bands and shifts of protein bands to 1,538, 1,650, and 3,303 cm^{-1} closely resemble the IR signature of hemoglobin-containing tissue [17, 20]. The IR spectrum of the class for other tissue differs significantly from IR spectra of normal brain tissue and astrocytic gliomas. Bands at 1,107, 1,248, 1,375, 1,445, 1,536, 1,650, 1,738, 2,851, 2,920, and 3,305 cm^{-1} point to tissue which is contaminated

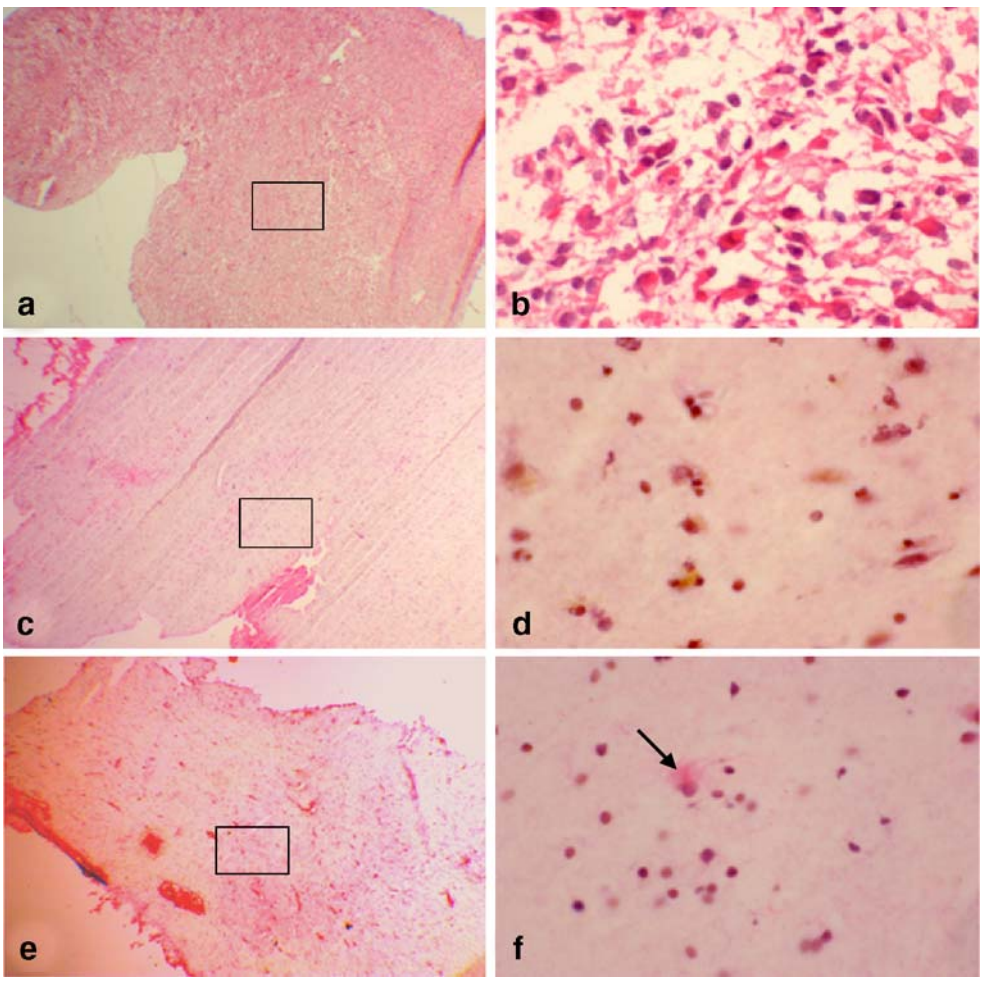

Fig. 5 Histomorphology of 5-µm-thick cryostat sections stained with hematoxylin and eosin. Low magnification overview of sections consecutive to Fig. 2a (**a**, high cellularity), to Fig. 3a (**c**, increased cellularity) and to Fig. 4a (**e**, regular cellularity). High magnification of the *boxed areas* in **a** (**b**), in **c** (**d**), and in **e** (**f**). Low magnification: original ×2, high magnification: original ×40f

by TFM. As the amide I intensities of these spectra were above the threshold of 0.15, these spectra were not removed from the data sets by the preprocessing procedure. The classification model was trained to identify these spectra as non-normal and non-tumor tissue. Less than 0.2% of all spectra are assigned to malignant gliomas. In contrast to the cryosections with more than 10% tumor areas in Figs. 2 and 3, further analyses would be required to confirm the presence of tumor cells. These analyses can involve IR microspectroscopic imaging or histopathology.

The histomorphology of 5-μm-thick, H&E-stained cryostat sections which are consecutive to the sections in Figs. 2, 3, 4 is shown in Fig. 5. An overview is given at low magnification, and details are presented at high magnification. Although the shape of each stained and unstained section is similar, a direct comparison is complicated due to different orientations. The coarse cellular, fibrous structure and high cell density are indicative of a malignant astroglial tumor, e.g., glioblastoma multiforme (Fig. 5a). At high magnification large polymorphic tumor cells with atypical nuclei and some necrotic areas are visible (Fig. 5b). Brain tissue with slightly increased cellularity (astrocytoma grade II) is shown in Fig. 5c. At high magnification few suspicious cells are evident which may represent astrocytic tumor cells. However, in a tumor which contains areas of obvious malignancy (Fig. 5b), areas of low cellularity with only few tumor cells do not represent a benign tumor astrocytoma grade II. Despite the morphologically benign appearance, these tumor cells may retain their malignant potential. As the chemical composition and the IR spectra seem to be similar for both tissue types, the LDA model assigns them to one class. Figure 5e shows a mostly regular pattern of brain tissue with some blood vessels. The high magnification image shows a single suspicious astrocytic cell.

Conclusions

The current study applied a supervised classification model based on the LDA algorithm to IR images of three specimens from one patient. The first cryosection contained on average 95% malignant glioma which points to a location within the tumor. The smaller percentage of 12–34% malignant gliomas and increased cell density are consistent with a location of the second cryosection near the tumor margins. Only single suspicious tumor cells within mostly normal brain tissue of regular cellularity were detected in the third cryosection which most likely originated from outside of the tumor. The high accuracy of the LDA model which was trained by IR spectra from different patients and with different detectors demonstrated that (i) the chemical information which is described by the selected descriptors is identical in IR spectra which were recorded by multi-channel or single-channel IR detectors, (ii) the spectral fingerprints used to distinguish normal brain tissue and tumors are conserved among patients, and (iii) the LDA model is able to describe and recognize these spectral patterns. The chemical and molecular differences between normal brain tissue and brain tumors are sufficiently large and the algorithm is robust enough so physical effects due to different detection systems do not seem to affect the accuracy of the classification model. More samples will be studied to further validate the model and to refine it by including more tissue classes and more descriptors if necessary. The observation that unknown IR spectra are assigned to a separate class suggests that the classes for normal brain tissue, astrocytic gliomas, and hemorrhage have already been well defined. The new IR spectra with atypical properties include impurities (Fig. 2), TFM (Fig. 4), and leptomeninges [17].

Rapid assessment of extended, inhomogeneous tissue samples constitutes a challenge for IR spectroscopic-based techniques. Single IR spectra or IR microspectroscopic images can only probe small areas in a reasonable time frame. Consequently, the problem arises that selection of small areas could miss important information, e.g., the detection of tumor cells outside the probed region. IR macrospectroscopic imaging can rapidly screen whole samples in the mm^2 up to the cm^2 range. Unfortunately, the spatial resolution of 63 μm is too low to probe details of the morphological information. However, IR spectroscopy probes the molecular fingerprint which is an independent tissue property. In the future, this new parameter might be able to describe additional features such as the aggressiveness of the tumor and the prognosis for the patient. Long-term studies and a larger number of specimens are required for such a prediction which is currently not available from the morphology. If data accumulation is significantly accelerated, higher resolution in the cellular range might be considered for rapid screening of these samples.

Acknowledgements This work is financially supported by the Volkswagen Foundation within the project "Molecular Endospectroscopy" of the program "Junior research groups at universities". The authors thank P.R. Griffith (University of Idaho, USA) for valuable suggestions to improve the manuscript.

References

1. Kleihus P, Cavenee WK (2000) Pathology and genetics of tumors of the nervous system. IARC Press, Lyon
2. Diem M, Romeo M, Boydston-White S, Miljkovic M, Matthäus C (2004) Analyst 129:880–885
3. Dukor RK (2002) In: Chalmers JM, Griffiths PR (eds) Handbook of vibrational spectroscopy. Wiley, Chichester, pp 3335–3361

4. Shaw RA, Mantsch HH (2000) In: Meyers RA (ed) Encyclopedia of analytical chemistry, vol 1. Wiley, Chichester, pp 83–102
5. Lasch P, Boese M, Pacifico A, Diem M (2002) Vib Spectrosc 28:147–157
6. Krafft C, Salzer R, Soff G, Meyer-Hermann M (2005) Cytometry A 64A:53–61
7. Steller W, Einenkel J, Horn LC, Braumann UD, Binder H, Salzer R, Krafft C (2006) Anal Bioanal Chem 384:145–154
8. Levin IW, Baghava R (eds) (2005) Spectrochemical analysis using infrared multichannel detectors. Blackwell Publishing Professional, Ames
9. Fabian H, Choo LP, Szendrei GI, Jackson M, Halliday WC, Otvös LJ, Mantsch HH (1993) Appl Spectrosc 47:1513–1518
10. Kretlow A, Wang Q, Kneipp J, Lasch P, Beekes M, Miller L, Naumann D (2006) BBA Biomem 1758:948–959
11. Bambery KR, Schültke E, Wood BR, Rigley MacDonald ST, Ataelmannan K, Griebel RW, Juurlink BHJ, McNaughton D (2006) BBA Biomem 1758:900–907
12. Amharref N, Beljebbar A, Dukic S, Venteo L, Schneider L, Pluot M, Vistelle R, Manfait M (2006) BBA Biomem 1758:892–899
13. Krafft C, Shapoval L, Sobottka SB, Schackert G, Salzer R (2006) Technol Cancer Res Treatm 5:291–298
14. Krafft C, Shapoval L, Sobottka SB, Geiger KD, Schackert G, Salzer R (2006) BBA Biomem 1758:883–891
15. Steiner G, Shaw A, Choo-Smith LP, Abuid MH, Schackert G, Sobottka S, Steller W, Salzer R, Mantsch HH (2003) Biopolymers 76:464–471
16. Beleites C, Steiner G, Sowa MG, Baumgartner R, Sobottka S, Schackert G, Salzer R (2005) Vib Spectrosc 38:143–149
17. Krafft C, Thümmler K, Sobottka SB, Schackert G, Salzer R (2006) Biopolymers 82:301–305
18. Kiefte M. Discrim Toolbox, available at http://www.mathworks.com
19. Krafft C, Sobottka SB, Schackert G, Salzer R (2004) Analyst 129:921–925
20. Krafft C, Sobottka SB, Schackert G, Salzer R (2006) J Raman Spectrosc 37:367–375